Journal of Computational Acoustics, Vol. 16, No. 3 (2008) 343–359

INTERNATIONAL ASSOCIATION
FOR MATHEMATICS AND
COMPUTERS IN SIMULATION

DEVELOPMENT OF A THREE-POINT SIXTH-ORDER HELMHOLTZ SCHEME

TONY W. H. SHEU*, L. W. HSIEH and C. F. CHEN

Department of Engineering Science and Ocean Engineering
National Taiwan University, No. 1, Sec. 4, Roosevelt Road
Taipei, Taiwan 10617, Republic of China
**twhsheu@ntu.edu.tw*

Received 8 December 2005
Revised 21 June 2007

A compact finite-difference scheme is presented in this paper for efficiently solving the variable Helmholtz equation. This scheme development involves relating the derivative terms, namely, u_{xx} and u_{xxxx}, to u at the two adjacent nodal points in order to yield a 3-point stencil implicit scheme. In addition to sixth-order accuracy, the proposed scheme can conditionally provide oscillation-free solutions using the underlying M-matrix theory. Computations have been carried out for several problems which are amenable to exact solutions. Agreement with the exact solutions is excellent even in a grid system involving fewer number of mesh points. Thus, the integrity of the compact scheme and the efficiency of the alternating direction implicit algorithm are demonstrated. The proposed scheme is applied to study the effect of variable wave number on the wave propagation characteristics for the problem, which is partly bounded by a scatter surface.

Keywords: Compact finite-difference scheme; Helmholtz equation; sixth-order accuracy; oscillation-free; M-matrix.

1. Introduction

Investigation of the Helmholtz equation is worthwhile as it is closely related to various scientific applications. Typical examples include the water wave propagation in the coastal regions,[1] the scattering wave from an elastic body,[2] and the sound wave propagation in water. A rule of thumb indicated in the numerical simulation of Helmholtz equation demands 10 mesh points per wavelength.[3] This constraint precludes a practical application since the physical domain can have a length that is thousand times of the wavelength. Under these circumstances, the amount of computer resources (CPU, I/O, memory, and disk storage) required for the implicit scheme becomes prohibitively large. This is a serious impediment to the use of conventional approaches, thereby motivating the development of two higher-order Helmholtz discretization schemes.

*Corresponding author.

High-order Helmholtz schemes can be constructed by introducing more number of finite-difference stencil points. These schemes can simultaneously increase the matrix bandwidth and are, thus, computationally more expensive. We are, therefore, motivated to develop a compact scheme so as to retain good prediction accuracy without involving many number of finite-difference stencil points. Since the tri-diagonal Thomas direct solver[4] is known to be cost-effective in the calculation of matrix equation, it is desirable that higher-order schemes can be formulated within the framework which involves only three stencil points.

When the multi-dimensional exterior acoustic problem is considered, the peripheral storage required for the matrix equation can be excessive and typically exceeds the available computer resources. To overcome this difficulty, the alternating direction implicit (ADI) method[5] is adopted in the present study. The benefit of employing the ADI method is that the tri-diagonal matrix solver[4] can be applied in each spatial sweep.

The remainder of this paper is organized as follows. In Sec. 2, the model differential equation is described. In Sec. 3, the newly developed fourth- and sixth-order accurate schemes are presented in detail. A rigorous theory will be employed to construct an M-matrix type scheme.[6,7] This is followed by verifying the proposed compact schemes via the three chosen problems which are amenable to exact solutions. Encouraged by the success in validating the Helmholtz scheme, in Sec. 5 the sixth-order compact scheme is applied to simulate the point-source wave propagation. Finally, some concluding remarks are provided in Sec. 6.

2. Model Equation

Numerical simulation of underwater acoustics often involves solving the following Helmholtz equation for the static pressure p:

$$\nabla^2 p + k^2(\mathbf{x})\, p = f(\mathbf{x}). \tag{1}$$

The real-valued variable k, known as the wave number, is allowed to vary with $\mathbf{x}$. In Eq. (1), f denotes the prescribed sound source. In order to make the above elliptic-type differential equation well-posed, it is solved subject to the conditions prescribed over the entire boundary of the physical domain.

When the Helmholtz equation for the underwater acoustics is solved, generally not less than 10 nodal points per wavelength[1] are needed to retain the predicted accuracy. The resulting consequence is that the problem will become prohibitively large. Therefore, we are motivated to develop two schemes which can yield high-order prediction accuracy in a domain discretized by fewer grid points so as to gain the computational efficiency.

3. Numerical Model for the Helmholtz Equation

For the proposed method, the following prototype equation is considered:

$$u_{xx} + k^2(x)\, u = f(x). \tag{2}$$

Inspired by the work of Lele,[8] a class of compact finite-difference schemes is developed, which will be presented in the subsequent sections.

3.1. *Fourth-order scheme*

Let us denote the approximation of u_{xx} at a point j as

$$u_{xx}|_j = s_j. \tag{3}$$

The scheme development is followed by relating the nodal value of $u_{xx}(x_j)$ to its two adjacent values $u_{xx}|_{j\pm1}$ as follows:

$$h^2(\beta_1 s_{j+1} + \beta_0 s_j + \beta_{-1} s_{j-1}) = \alpha_1 u_{j+1} + \alpha_0 u_j + \alpha_{-1} u_{j-1}. \tag{4}$$

In the above equation, h denotes the grid size. With the definition mentioned in the Eq. (3), the following equations are obtained:

$$\begin{aligned} s_{j+1} + k_{j+1}^2 u_{j+1} &= f_{j+1}, \\ s_j + k_j^2 u_j &= f_j, \\ s_{j-1} + k_{j-1}^2 u_{j-1} &= f_{j-1}. \end{aligned} \tag{5}$$

By substituting Eqs. (5) into Eq. (4), we get

$$\begin{aligned} &(\alpha_1 + h^2 k_{j+1}\beta_1) u_{j+1} + (\alpha_0 + h^2 k_j \beta_0) u_j + (\alpha_{-1} + h^2 k_{j-1}\beta_{-1}) u_{j-1} \\ &\quad = h^2(\beta_1 f_{j+1} + \beta_0 f_j + \beta_{-1} f_{j-1}). \end{aligned} \tag{6}$$

To make u amenable to a tri-diagonal matrix equation solver, the six free parameters shown in Eq. (6) have to be determined. These six parameters α_0, β_0, $\alpha_{\pm1}$, and $\beta_{\pm1}$ are determined by expanding $s_{j\pm1}$ with respect to s_j while expanding $u_{j\pm1}$ with respect to u_j. After some algebra, the following equation is obtained:

$$\begin{aligned} s_j = \frac{1}{h^2(\beta_1 + \beta_0 + \beta_{-1})} \Bigg\{ &(\alpha_1 + \alpha_0 + \alpha_{-1}) u_j + h(\alpha_1 - \alpha_{-1}) u^{(1)}|_j + \frac{h^2}{2!}(\alpha_1 + \alpha_{-1}) u^{(2)}|_j \\ &+ \left[\frac{h^3}{3!}(\alpha_1 - \alpha_{-1}) - h^3(\beta_1 - \beta_{-1})\right] u^{(3)}|_j + \left[\frac{h^4}{4!}(\alpha_1 + \alpha_{-1}) - \frac{h^4}{2!}(\beta_1 + \beta_{-1})\right] u^{(4)}|_j \\ &+ \left[\frac{h^5}{5!}(\alpha_1 - \alpha_{-1}) - \frac{h^5}{3!}(\beta_1 - \beta_{-1})\right] u^{(5)}|_j + \left[\frac{h^6}{6!}(\alpha_1 + \alpha_{-1}) - \frac{h^6}{4!}(\beta_1 + \beta_{-1})\right] u^{(6)}|_j \Bigg\}. \end{aligned} \tag{7}$$

By virtue of Eq. (3), the following six equations can be derived

$$\begin{aligned} \alpha_1 + \alpha_0 + \alpha_{-1} &= 0, \\ \alpha_1 - \alpha_{-1} &= 0, \\ \alpha_1 + \alpha_{-1} &= 2(\beta_1 + \beta_0 + \beta_{-1}), \\ \frac{1}{6}(\alpha_1 - \alpha_{-1}) - \beta_1 + \beta_{-1} &= 0, \\ \frac{1}{12}(\alpha_1 + \alpha_{-1}) - \beta_1 - \beta_{-1} &= 0, \\ \frac{1}{20}(\alpha_1 - \alpha_{-1}) - \beta_1 + \beta_{-1} &= 0. \end{aligned} \tag{8}$$

Calculation of the above coupled equations results in $\alpha_1 : \alpha_0 : \alpha_{-1} : \beta_1 : \beta_0 : \beta_{-1} = 12 : -24 : 12 : 1 : 10 : 1$. These free parameters are then substituted into Eq. (6) to derive the discrete equation, which is given below, for the model equation given in Eq. (2):

$$(12 + h^2k_{j+1}^2)u_{j+1} - 2(12 - 5h^2k_j^2)u_j + (12 + h^2k_{j+1}^2)u_{j-1} = h^2(f_{j+1} + 10f_j + f_{j-1}). \tag{9}$$

To understand the proposed discrete equation (2), $u_{j\pm1}$ are expanded with respect to u_j and then substituted into Eq. (9) to derive the following modified equation[9]:

$$\begin{aligned} k^2u + u_x = f &- \frac{h^2}{12}\{[2(kk_{xx} + k_x^2)u + 4kk_xu_x + (k^2u_{xx} + u_{xxxx})] - f_{xx}\} \\ &- \frac{h^4}{12}\left[\frac{1}{6}(3k_{xx}^2 + kk_{xxxx} + 4k_xk_{xxx})u + 2\left(k_xk_{xx} + \frac{1}{3}kk_{xxx}\right)u_x\right. \\ &\left. + (kk_{xx} + k_x^2)u_{xx} + \frac{4}{3!}(kk_x)u_{xxx} + \frac{2}{4!}(k^2)u_{xxxx} + \cdots\right] + \frac{h^4}{12}f_{xxxx} + \text{H.O.T.} \end{aligned} \tag{10}$$

Since $\partial^2/\partial x^2(k^2u + u_{xx}) = 2(kk_{xx} + k_x^2)u + 4kk_xu_x + (k^2u_{xx} + u_{xxxx}) = f_{xx}$, Eq. (10) is rewritten as

$$\begin{aligned} k^2u + u_x = f &- \frac{h^2}{12}\left[\frac{1}{6}(3k_{xx}^2 + kk_{xxxx} + 4k_xk_{xxx})u + 2\left(k_xk_{xx} + \frac{1}{3}kk_{xxx}\right)u_x\right. \\ &\left. + (kk_{xx} + k_x^2)u_{xx} + \frac{4}{3!}(kk_x)u_{xxx} + \frac{2}{4!}(k^2)u_{xxxx} + \cdots\right] + \frac{h^4}{12}f_{xxxx} + \text{H.O.T.} \end{aligned} \tag{11}$$

The above equation reveals that the right-hand side approaches zero as the grid size h is decreased. This implies that the three-point stencil scheme accommodates the consistency property. Since any implicit scheme is unconditionally stable, the numerical results exhibiting the convergence property can be expected in lieu of the Lax's equivalent theorem.[10] Based on the above modified equation analysis, the accuracy order for the proposed scheme involving only three stencil points is $O(h^4)$.

3.2. *Sixth-order scheme*

To further improve the prediction accuracy, we can, of course, introduce more stencil points to the discrete formulation. The improved prediction accuracy is, however, obtained at the cost of an increasingly expensive calculation of matrix equation. To retain the prediction accuracy at a lower computational cost, we are motivated to develop a scheme that has an accuracy order of up to six in a grid involving only three points. Now, another auxiliary variable t at x_j is introduced and is shown below:

$$u_{xxxx}|_j = t_j. \tag{12}$$

Development of the compact scheme at x_j begins with relating t and s with u as follows:

$$h^4(\gamma_1 t_{j+1} + \gamma_0 t_j + \gamma_{-1} t_{j-1}) + h^2(\beta_1 s_{j+1} + \beta_0 s_j + \beta_{-1} s_{j-1}) = \alpha_1 u_{j+1} + \alpha_0 u_j + \alpha_{-1} u_{j-1}. \tag{13}$$

Further derivation is followed by expanding $t_{j\pm1}$, $s_{j\pm1}$ and $u_{j\pm1}$ with respect to t_j, s_j, and u_j, respectively. Substituting these Taylor-series expansion equations into Eq. (13), we get

$$\begin{aligned}
&h^4(\gamma_1+\gamma_0+\gamma_{-1})t_j + h^5(\gamma_1-\gamma_{-1})t_x + \frac{h^6}{2!}(\gamma_1+\gamma_{-1})t_{xx} \\
&\quad + h^2(\beta_1+\beta_0+\beta_{-1})s_j + h^3(\beta_1-\beta_{-1})s_x + \frac{h^4}{2!}(\beta_1+\beta_{-1})s_{xx} \\
&\quad + \frac{h^5}{3!}(\beta_1-\beta_{-1})s^{(3)} + \frac{h^6}{4!}(\beta_1+\beta_{-1})s^{(4)} \\
&= (\alpha_1+\alpha_0+\alpha_{-1})u_j + h(\alpha_1-\alpha_{-1})u_x + \frac{h^2}{2!}(\alpha_1+\alpha_{-1})u_{xx} \\
&\quad + \frac{h^3}{3!}(\alpha_1-\alpha_{-1})u^{(3)} + \frac{h^4}{4!}(\alpha_1+\alpha_{-1})u^{(4)} + \frac{h^5}{5!}(\alpha_1-\alpha_{-1})u^{(5)} \\
&\quad + \frac{h^6}{6!}(\alpha_1+\alpha_{-1})u^{(6)} + \frac{h^7}{7!}(\alpha_1-\alpha_{-1})u^{(7)} + \frac{h^8}{8!}(\alpha_1+\alpha_{-1})u^{(8)}.
\end{aligned} \tag{14}$$

A term-by-term comparison of the derivatives shown in Eq. (14) leads to eight simultaneous algebraic equations, from which the introduced free parameters can be determined as $\alpha_1 = \alpha_{-1} = -5040$, $\beta_1 = \beta_{-1} = -660$, $\gamma_1 = \gamma_{-1} = 41$, $\alpha_0 = 10\,080$, $\beta_0 = -3720$, and $\gamma = 158$. Note that $t_m = (k_m^4 - 2k_{x,m}^2 - 2k_m k_{xx,m})u_m - k_m^2 f_m - 4k_m k_{x,m} u_{x,m}$ and $s_m = -k_m^2 u_m + f_m$ $(m = j, j \pm 1)$. Equation (14) can be expressed as

$$\begin{aligned}
&[\alpha_1 + \beta_1 h^2 k_{j+1}^2 - \gamma_1 h^4 (k_{j+1}^4 - 2k_{x,j+1}^2 - 2k_{j+1}k_{xx,j+1})]u_{j+1} \\
&\quad + [\alpha_0 + \beta_0 h^2 k_j^2 - \gamma_0 h^4 (k_j^4 - 2k_{x,j}^2 - 2k_j k_{xx,j})]u_j \\
&\quad + [\alpha_{-1} + \beta_{-1} h^2 k_{j-1}^2 - \gamma_{-1} h^4 (k_{j-1}^4 - 2k_{x,j-1}^2 - 2k_{j-1}k_{xx,j-1})]u_{j-1} \\
&= h^4(-4\gamma_1 k_{j+1} k_{x,j+1} u_{x,j+1} - 4\gamma_0 k_j k_{x,j} u_{x,j} - 4\gamma_{-1} k_{j-1} k_{x,j-1} u_{x,j-1}) \\
&\quad + h^2[(\beta_1 - \gamma_1 h^2 k_{j+1}^2) f_{j+1} + (\beta_0 - \gamma_0 h^2 k_j^2) f_j + (\beta_{-1} - \gamma_{-1} h^2 k_{j-1}^2) f_{j-1}] \\
&\quad + h^4(\gamma_1 f_{xx,j+1} + \gamma_0 f_{xx,j} + \gamma_{-1} f_{xx,j-1}).
\end{aligned} \tag{15}$$

It is noted that the above equation is derived subject to the condition given by

$$h(c_1 r_{j+1} + c_0 r_j + c_{-1} r_{j-1}) = (a_1 u_{j+1} + a_0 u_j + a_{-1} u_{j-1}) + h^2(b_1 s_{j+1} + b_0 s_j + b_{-1} s_{j-1}), \tag{16}$$

where $r \equiv u_x$, $c_1 = -4h^3 k_{j+1} k_{x,j1} \gamma_1$, $c_0 = -4h^3 k_j k_{x,j} \gamma_0$ and $c_{-1} = -4h^3 k_{j-1} k_{x,j-1} \gamma_{-1}$. Following the same approach described above for the fourth-order compact scheme, the

coefficients for $a_{\pm1,0}$ and $b_{\pm1,0}$ are obtained as

$$\begin{aligned} a_1 &= \frac{1}{2}(c_1 + 3c_0 - 7c_{-1}), \\ a_0 &= -2c_0 + 8c_{-1}, \\ a_{-1} &= -\frac{1}{2}(c_1 - c_0 + 9c_{-1}), \\ b_1 &= \frac{1}{6}(2c_1 - c_0 + 2c_{-1}), \\ b_0 &= \frac{1}{6}(4c_1 - 5c_0 + 16c_{-1}), \\ b_{-1} &= 0. \end{aligned} \tag{17}$$

By substituting Eq. (16) along with coefficients shown in Eq. (17) into Eq. (15), it follows that

$$\begin{aligned} &[-5040 - 660h^2k_{j+1}^2 - 41h^4(k_{j+1}^4 - 2k_{x,j+1}^2 - 2k_{j+1}k_{xx,j+1}) - a_1 + b_1h^2k_{j+1}^2]u_{j+1} \\ &\quad + [10\,080 - 3720h^2k_j - 158h^4(k_j^4 - 2k_{x,j}^2 - 2k_jk_{xx,j}) - a_0 + b_0h^2k_j^2]u_j \\ &\quad + [-5040 - 660h^2k_{j-1}^2 - 41h^4(k_{j-1}^4 - 2k_{x,j-1}^2 - 2k_{j-1}k_{xx,j-1}) - a_{-1} + b_{-1}h^2k_{j-1}^2]u_{j-1} \\ &= -h^2[(660 + 41h^2k_{j+1}^2 - b_1)f_{j+1} + (3720 + 158h^2k_j^2 - b_0)f_j \\ &\quad + (660 + 41h^2k_{j-1}^2 - b_{-1})f_{j-1}] + h^4(41f_{xx,j+1} + 158f_{xx,j} + 41f_{xx,j-1}). \end{aligned} \tag{18}$$

Here, $c_1 = -164h^3k_{j+1}k_{x,j+1}$, $c_0 = -632h^3k_jk_{x,j}$, and $c_{-1} = -164h^3k_{j-1}k_{x,j-1}$ are invoked in the derivation of Eq. (18). At the constant wave number limiting condition, the corresponding modified equation for the proposed scheme is derived as follows after some algebra:

$$k^2u + u_{xx} = h^6\left(\frac{19k^2}{60\,480} - \frac{477k^4}{12\,700\,800}h^2 + \cdots\right)u^{(6)} + \cdots + \text{H.O.T.} \tag{19}$$

This modified equation analysis demonstrates that the scheme developed within the three-point stencil framework can yield a prediction accuracy of order 6. The apparent advantage is that the Helmoholtz solution can be obtained easily by employing a tri-diagonal solution solver.[4]

3.3. *Constraint on the solution monotonicity*

Acoustics are featured with a highly fluctuating pressure field. It is, thus, important to clarify whether the predicted oscillating pressure solution is physically relevant or is numerically produced, especially when a highly accurate scheme is applied to solve the problems involving high-frequency sound sources. In this study, we will employ the M-matrix theory[6,7]

to solve for the physically relevant wavy solution. Some definitions and theorems useful to construct the monotonic scheme are given below[6,7]:

Definition 3.1. A real $n \times n$ matrix $\mathbf{A}\,(= a_{ij})$ is classified as being irreducible diagonally dominant if $|a_{ij}| > \sum_{ij=1, i\neq j}^{n} |a_{ij}|$ for at least one i.

Definition 3.2. A real $n \times n$ matrix $\mathbf{A}\,(= a_{ij})$ with $a_{ij} \leq 0$ for all $i \neq j$ is called M-matrix if $\mathbf{A}$ is non-singular and $\mathbf{A}^{-1} > 0$.

Definition 3.3. A real $n \times n$ matrix $\mathbf{A}$ is defined as monotonic provided that $\mathbf{A}\psi \geq 0$ holds for any vector ψ under the condition $\psi \geq 0$.

Theorem 3.1. *If a real and irreducible diagonally dominant matrix has the properties, namely,* $a_{ij} \leq 0$ *for* $i \neq j$ *and* $a_{ii} > 0$ *for* $1 \leq i \leq n$, *then* $\mathbf{A}^{-1} > 0$.

Theorem 3.2. *If the off-diagonal entries of* $\mathbf{A}$ *are nonpositive, then* $\mathbf{A}$ *is termed as a monotone matrix if and only if* $\mathbf{A}$ *is an M-matrix.*

For example, consider the constant wavenumber case; the two proposed implicit schemes are monotonic provided that the diagonal coefficient a_j has a positive value. Under these circumstances, $a_{j\pm1}$ are unconditionally negative in magnitude. By applying the theorems pertaining to the solution monotonicity, the validity of the two proposed compact monotonic schemes are subjected to the respective conditions given below:

(a) fourth-order scheme

$$5(hk)^2 - 12 \leq 0 \quad (\text{or } hk < 1.549); \tag{20}$$

(b) sixth-order scheme

$$79(hk)^4 + 1860(hk)^2 - 5040 \leq 0 \quad (\text{or } hk < 1.566). \tag{21}$$

For the sake of comparison, the monotonic constraint condition, namely, $(hk)^2 - 2 \leq 0$ (or $hk < 1.414$), for the centered scheme is also derived. Depending on the wave number k, the grid size chosen to obtain the monotonic solution should fall into the shaded areas depicted in Fig. 1. Characterized by the current two compact schemes, the monotonic region increases in size with the increased accuracy order.

The fourth- and sixth-order accurate compact schemes developed in Cartesian grids can be extended to simulate the practical problems with complex geometries by different means. One can rewrite the working equation cast in curvilinear physical coordinates to the orthogonal computational coordinates and solve the resulting transformed equation in Cartesian coordinates using the proposed compact schemes.[11] One can also apply the immersed boundary method (IBM), which adds a properly derived source term to the working equation, and apply the proposed compact scheme to solve the Helmholtz equation, defined in irregular domain, in Cartesian grids. The idea of IBM is to derive the source

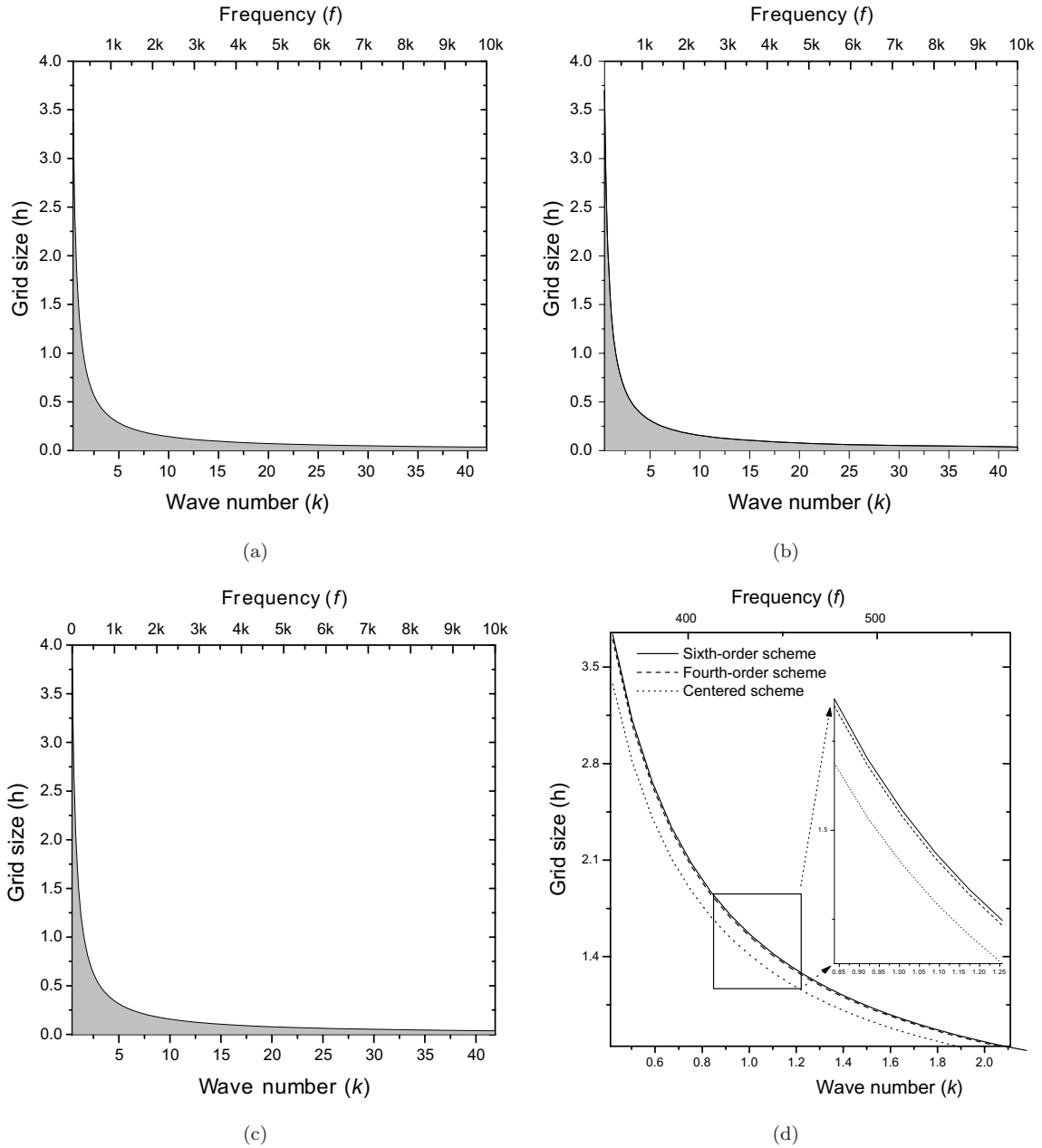

Fig. 1. Schematic of the monotonic range of $k-h$ (or $f-h$) in the shaded area. (a) centered scheme; (b) fourth-order scheme; (c) sixth-order scheme; (d) a direct comparison of the monotonic regions plotted in (a), (b), and (c). Here, f is computed at the chosen speed of sound $c = 1500\,\mathrm{m/s}$.

term in a way that the boundary condition prescribed along the irregular boundary can be approximately satisfied through the interpolation of nodal points in the vicinity of boundary nodes. The reader can refer to the work presented in Ref. 12 for the analysis of incompressible Navier–Stokes equations in complex geometry.

4. Verification of the Helmholtz Scheme

4.1. *Inhomogeneous one-dimensional validation case*

Validation of the proposed three-point Helmholtz schemes is made by considering the following cornerstone point-source problem in the area of underwater acoustics:

$$\phi_{xx} - k^2\phi = g\ell\delta(x-\eta). \tag{22}$$

In the above equation, δ is the delta function. The chosen test problem involves specification of two end boundary conditions given by $\phi(\ell) = \phi(-\ell) = 0$. Under the condition given by $-\ell \le \eta \le \ell$, the solution for Eq. (22) can be analytically derived as

$$\phi(x,k,\eta) = \begin{cases} -\dfrac{g\ell}{k}\dfrac{\sinh[k(\ell-\eta)]}{\sinh(2k\ell)}\sinh[k\,(\ell+x)] & -\ell < x < \eta, \\ -\dfrac{g\ell}{k}\dfrac{\sinh[k(\ell+\eta)]}{\sinh(2k\ell)}\sinh[k(\ell-x)] & -\eta < x < \ell. \end{cases} \tag{23}$$

The solution was obtained at $\eta = 0$, $\ell = 1$, $g = 1000$, and $k = 113$. For the case with a constant grid size of $h = 0.02$, it is found from Fig. 2 that the finite-difference solutions compare well with the analytical solution given in Eq. (23). The profile of ϕ can be sharply captured for the given value of k and the chosen grid size h, which follows Eq. (21).

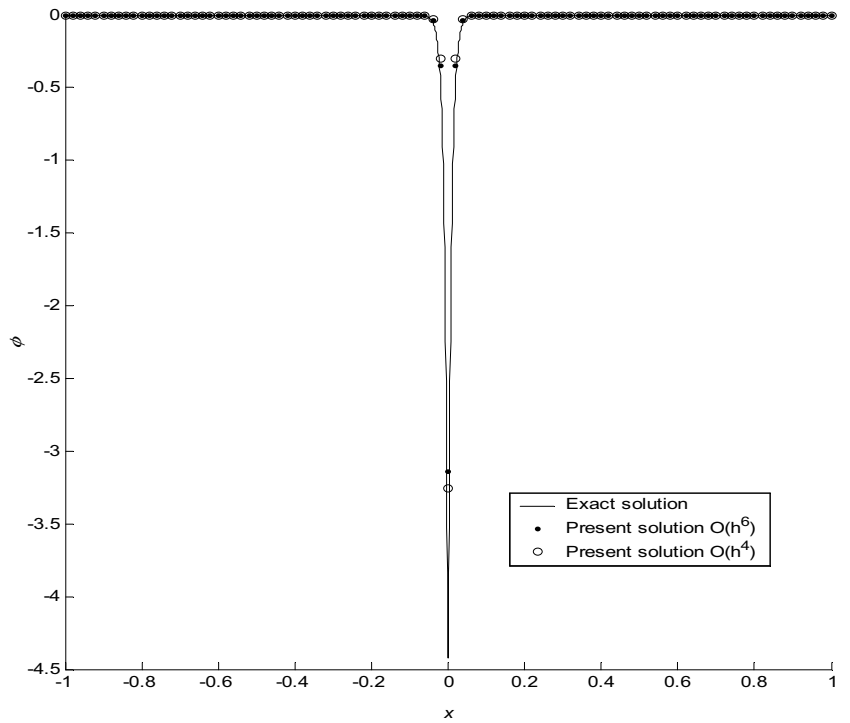

Fig. 2. A comparison of the fourth- and sixth-order compact solutions with the exact solution given in Eq. (3).

4.2. *One-dimensional validation — Variable wave number case*

After the successful validation of the present scheme, the following variable wave number case is then considered

$$u_{xx} + \sin^2(x)u = \sin^3(x) - \sin(x) \quad 0 \le x \le 20. \tag{24}$$

Subjected to $u(0) = 0$ and $u(20) = \sin(20)$, Eq. (24) has the following exact solution:

$$u_{\text{exact}} = \sin(x). \tag{25}$$

The results obtained at $\Delta x = 20/17$ are shown in Fig. 3. It is seen that the predicted solutions follow the trend of the theoretical results, thus verifying the two proposed Helmholtz schemes. For the sake of comparison, the solution obtained by using the centered scheme is also plotted in this figure. It is evident that the proposed sixth-order scheme outperforms the conventional second-order centered scheme and the fourth-order compact scheme given in Eq. (9). A continuous increase of the grid points to 129 and 25 gives the results, which are obtained using the second- and fourth-order schemes, comparable to the sixth-order solutions obtained at 18 grid points. A considerable computational time is saved using the

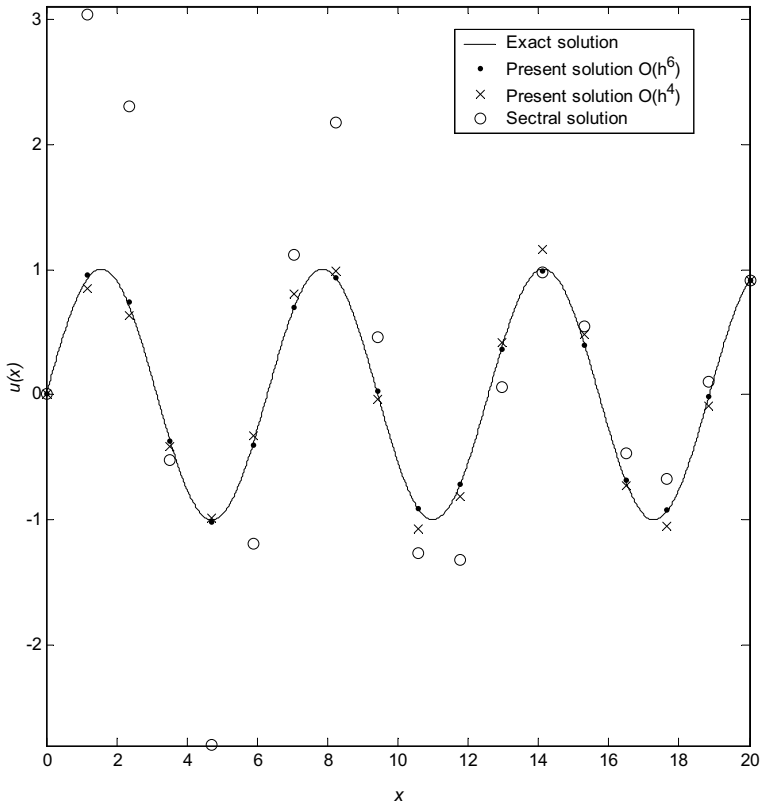

Fig. 3. A comparison of the fourth- and sixth-order compact solutions with the exact solution given in Eq. (5).

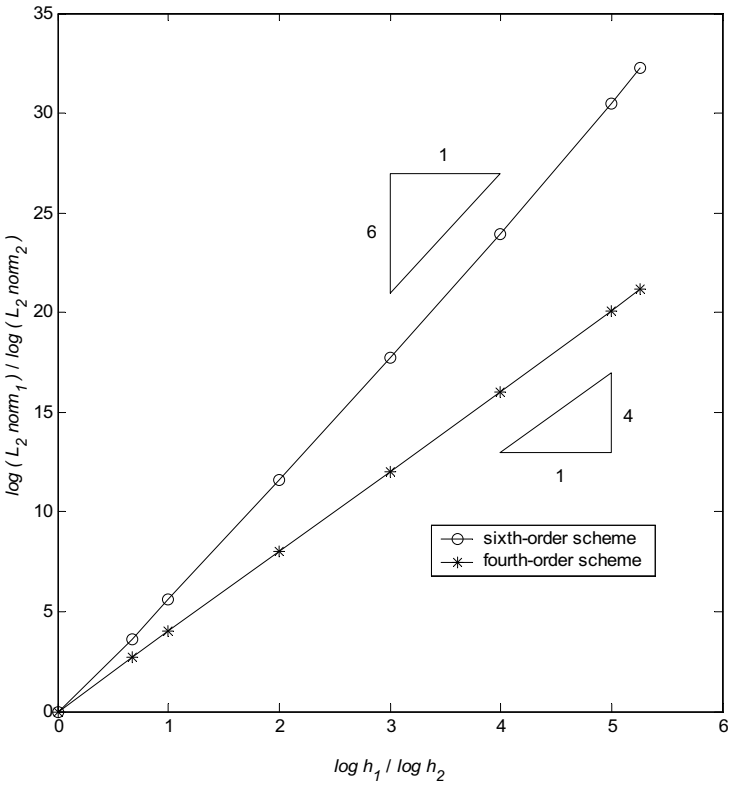

Fig. 4. The predicted rates of convergence for the variable Helmholtz equation considered in Sec. 4.2.

proposed compact fourth- and sixth-order schemes. For this reason, the computationally more efficient sixth-order compact scheme for the two-dimensional analysis is applied.

To verify that the compact schemes given in Eqs. (9) and (18), which provide the fourth- and the sixth-order accuracy, respectively, the rate of convergence test is conducted by carrying out the calculations on several continuously refined uniform grids. The computed errors were cast in their L_2-error norms. Let us denote err_i $(i = 1, 2)$ as the L_2-error norms obtained at two continuously refined grids, $(M_1 + 1)$ and $(M_1 + 2)$. By plotting the logarithm of L_2-error norms against the grid sizes, the rate of convergence is obtained as $c\,(\equiv \log(\mathrm{err}_1/\mathrm{err}_2)/\log(M_2/M_1))$. Figure 4 shows that as the slopes approach the values of 4 and 6, the two proposed three-point compact schemes can yield solutions with the accuracy orders of four and six, respectively.

4.3. *Two-dimensional verification — Constant wave number case*

The following two-dimensional problem is considered to justify the use of compact scheme, used in conjunction with the ADI approach, to solve for ϕ in $0 \le x, y \le \pi/2$:

$$\nabla^2\phi + 2\phi = 0. \tag{26}$$

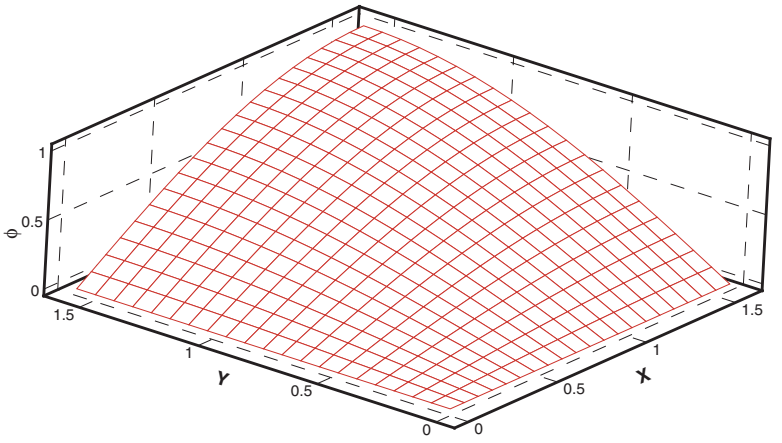

(a)

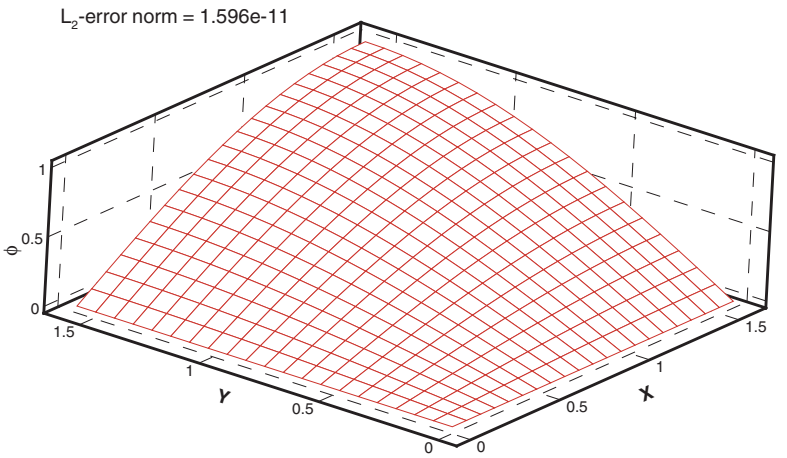

(b)

Fig. 5. A comparison of the predicted sixth-order compact solution profile with the exact profile of ϕ given in Eq. (27). (a) exact solution profile; (b) sixth-order accurate compact solution profile.

The above equation, subjected to the Dirichlet-type boundary condition for ϕ, is amenable to the following exact solution:

$$\phi(x, y) = \sin(x)\sin(y). \tag{27}$$

As Fig. 5 shows, the solution computed at $h = \pi/40$ agrees well with the exact solution given in Eq. (27). The computations in continuously refined grids, namely, $h = \pi/10$, $\pi/20$, $\pi/40$, $\pi/60$, $\pi/80$, are also performed and the prediction errors are computed in their L_2-norms. This was followed by plotting the values of $\log(\text{err}_1/\text{err}_2)$ against $\log(h_1/h_2)$ for the errors err_1 and err_2 predicted in the two continuously refined grids h_1 and h_2. As Fig. 6 shows, the rate of convergence was found to be 6 using the proposed sixth-order scheme.

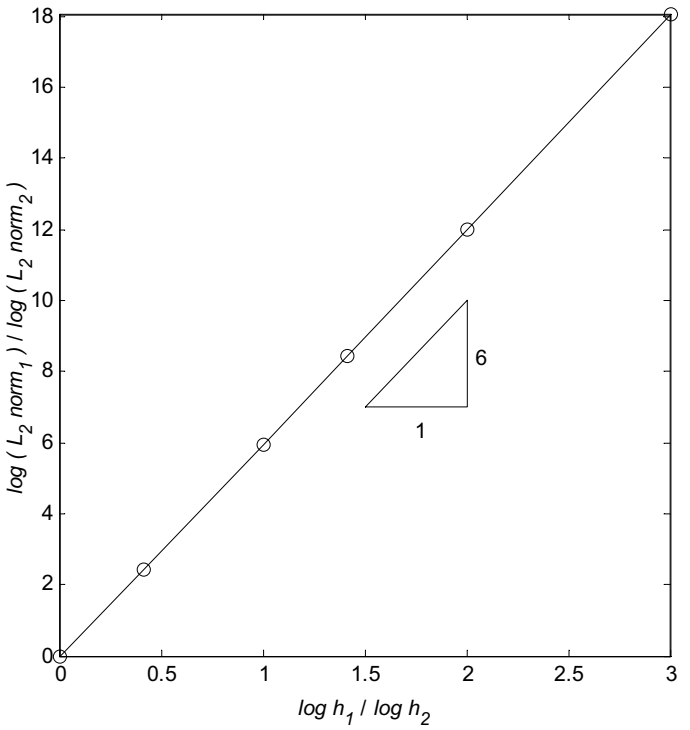

Fig. 6. The predicted rate of convergence for the two-dimensional Helmholtz equation considered in Sec. 4.3 using the sixth-order compact scheme.

5. Results and Discussions

Having verified the proposed three-point Helmholtz scheme and justified the use of the alternating direction implicit solution algorithm for the two-dimensional problem, the underwater acoustics in the presence of a point-source at $(0, y_0)$ is simulated. The physical problem is governed by the following differential equation for p:

$$\nabla^2 p + k^2 p = -\frac{\delta(\mathbf{r})}{2\pi}\,\delta(y - y_0). \tag{28}$$

In the above equation, $\mathbf{r}$ denotes the position vector pointing to the sound source. Here, the real wave number $k\,(\equiv 2\pi(\nu/c))$, where ν is the frequency of the sound source, of the positive sign varies with the sound propagation speed c.

In order to make Eq. (28) well-posed, it is imperative to prescribe the boundary value of p along the entire boundary of the domain. At infinity $(r \to \infty)$, it is rational to use the following Robin-type radiation boundary condition to minimize the nonphysical wave reflection from the open boundary:

$$\lim_{r\to\infty} \sqrt{r}\left(\frac{\partial p}{\partial r} - ikp\right) = 0. \tag{29}$$

At the free surface ($y = 0$), p is set to have the following fixed ambient pressure:

$$p(x, 0) = 0. \tag{30}$$

At the hard bottom, the Neumann-type boundary condition for p is prescribed as

$$\frac{\partial p(x, H)}{\partial y} = 0. \tag{31}$$

On the scatter surface $\partial\Omega$ schematically shown in Fig. 7, the pressure vanishes in the direction orthogonal to $\partial\Omega$. This implies that

$$\frac{\partial p}{\partial n} = 0. \tag{32}$$

To begin with, a point source having a frequency of $\nu = 1500\,\text{Hz}$ and a sound speed of $c = 1500\,\text{m/s}$ are considered. The sound source was placed below the flat free surface with a depth of $H = 4.2\,\text{m}$. The physical domain was defined in $0 \le x \le 4\,\text{m}$ and $0 \le y \le 4.2\,\text{m}$. The predicted ADI solution for p is said to be convergent if the maximum difference of solutions computed between x- and y-sweep fell below 10^{-6}. In this study, the calculations were performed on grids which were uniformly distributed with the grid sizes of $\Delta x = 0.1$ and $\Delta y = 0.1$.

The computed p is plotted in its contour-valued form in Fig. 8. To clearly illustrate the point-source produced pressure field, in Fig. 9 the contour values of p at several selected sections, namely, $x = 2$, $x = 3$, $y = 2.1$, and $y = 3.1$ are plotted. As these wavy pressures reveal, one can see the acoustic signature of the fixed frequency point source in the water.

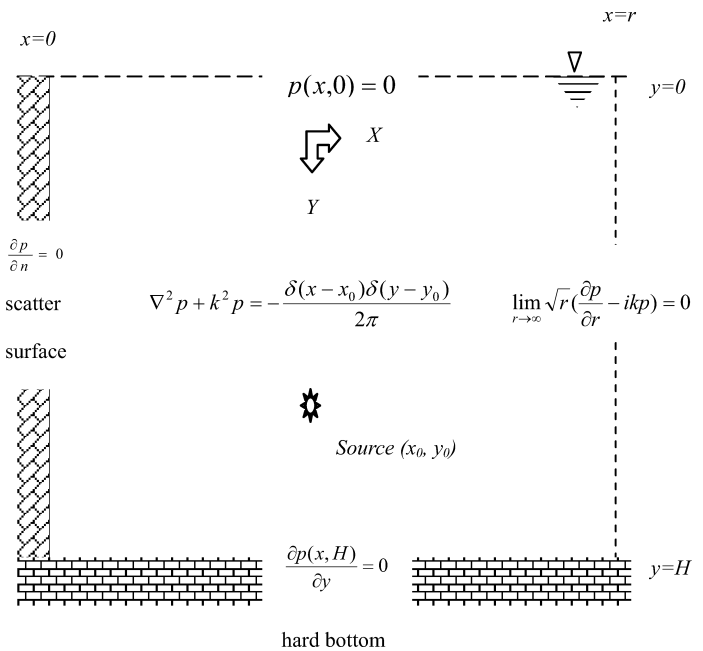

Fig. 7. Schematic of the sound source in the investigated domain which is bounded by four boundaries.

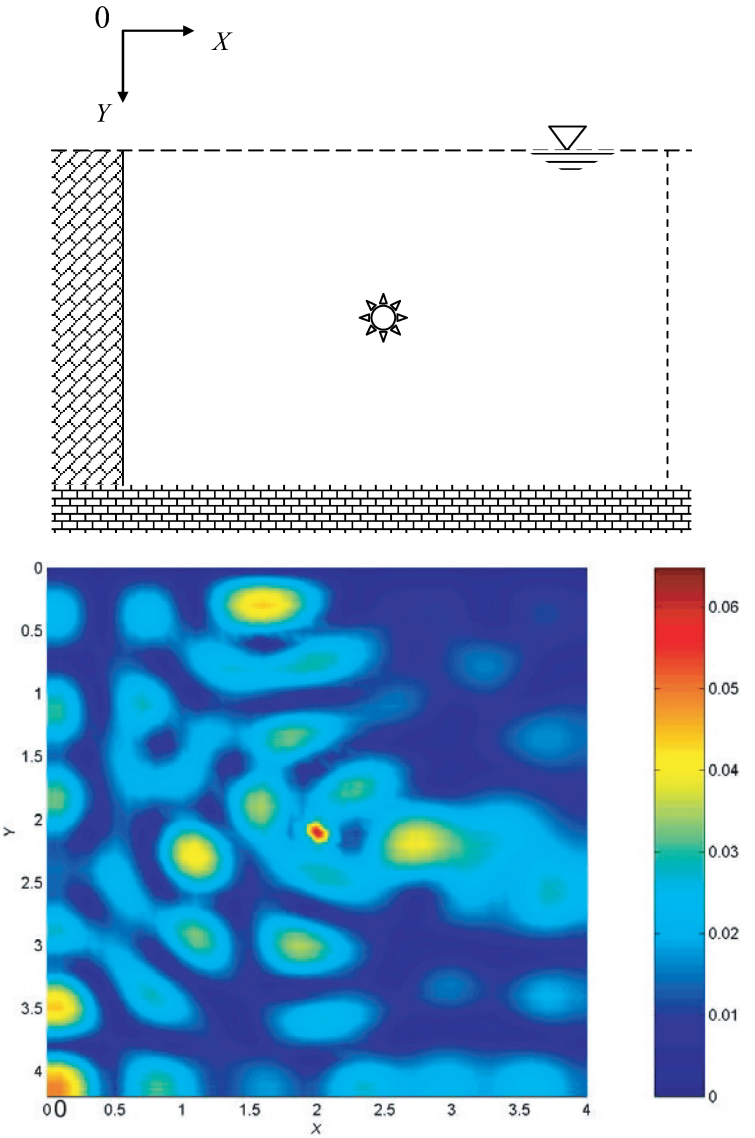

Fig. 8. The computed contour values of p for the scattering wave problem considered in Sec. 5.

6. Concluding Remarks

This paper has presented two compact finite-difference schemes for solving the Helmholtz equation. The emphasis has been placed on the improved prediction accuracy without adding more points to the finite-difference formulation. Our underlying idea is to relate the derivative terms with zero, second, and fourth orders. The Taylor series expansion has been used to determine the linearly independent coefficients shown in the finite-difference equation so that the three-point scheme has the accuracy orders of fourth and sixth. It is noteworthy that the grid sizes can be theoretically chosen to render an M-matrix equation. The

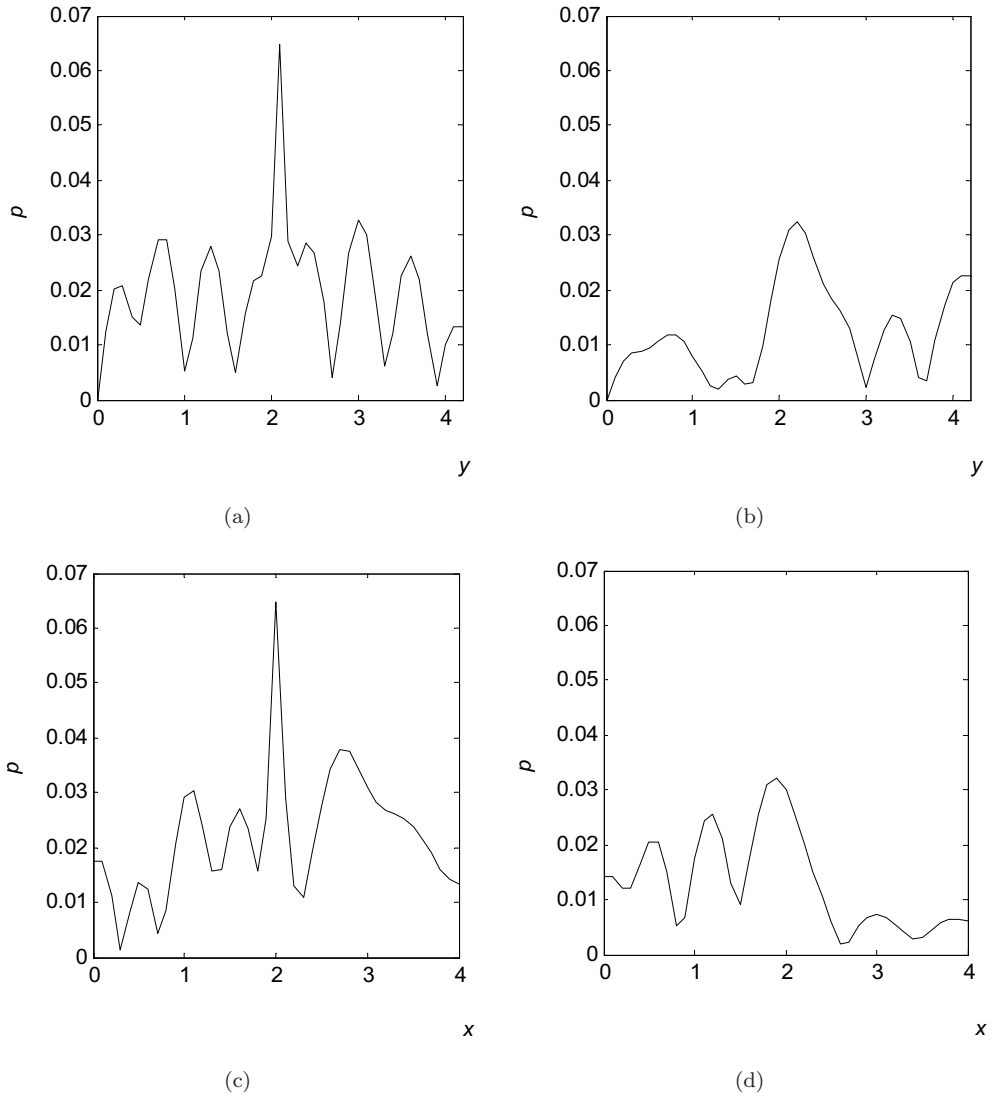

Fig. 9. The predicted pressure distributions at the four selected sections. (a) $x = 2$; (b) $x = 3$; (c) $y = 2.1$; (d) $y = 3.1$.

solution thus obtained can prevent any numerically generated oscillations to occur. Since the proposed scheme is new, analytical verification of the scheme has been conducted for both one- and two-dimensional problems. In conjunction with the ADI scheme of Polezhaev, the three-point sixth-order finite-difference scheme has been successfully applied to simulate the two-dimensional scattering wave problem.

References

1. F. S. B. F. Oliveira and K. Anastasiou, An efficient computational model for water wave propagation in coastal regions, *Appl. Ocean Res.* **20** (1998) 263–271.

2. I. Babŭska, F. Ihlenburg, E. T. Park and S. A. Sauter, A generalized finite element method for solving the Helmholtz equation in two dimensions with minimal pollution, *Comput. Methods Appl. Mech. Eng.* **128** (1995) 325–359.
3. P. Monk and D. Q. Wang, A least-squares method for the Helmholtz equation, *Comput. Methods Appl. Mech. Eng.* **175** (1999) 121–136.
4. L. H. Thomas, Elliptic problems in linear difference equations over a network, Watson Science Computer Laboratory Report (Columbia University, New York, 1949).
5. V. L. Polezhaev, Numerical solution of the system of two-dimensional unsteady Navier–Stokes equations for a compressible gas in a closed region, *Fluid Dynamics* **2** (1967) 70–74.
6. T. Ikeda, *Maximal Principle in Finite Element Methods for Convection-Diffusion Phenomena*, Lecture Notes in Numerical and Applied Analysis, Vol. 4 (North-Holland, Amsterdam, 1983).
7. T. Meis and U. Marcowitz, *Numerical Solution of Partial Differential Equations*, Applied Mathematical Science, Vol. 32 (Springer-Verlag, New York, 1981).
8. S. K. Lele, Compact finite difference schemes with spectral-like resolution, *J. Comput. Phys.* **103** (1992) 16–42.
9. R. F. Warming and B. J. Hyette, The modified equation approach to the stability and accuracy analysis of finite-difference methods, *J. Comput. Phys.* **14** (1974) 159–179.
10. P. D. Lax, Weak solutions of nonlinear hyperbolic equations and their numerical computation, *Commun. Pure Appl. Math.* **2** (1954) 159–193.
11. T. W. H. Sheu and S. M. Lee, A segrergated solution algorithm for incompressible flows in general co-ordinates, *Int. J. Numer. Meth. Fluids* **22** (1996) 1–34.
12. T. W. H. Sheu, H. F. Ting and R. K. Lin, An immersed boundary method for the incompressible Navier–Stokes equations in complex geometry, *Int. J. Numer. Meth. Fluids* **56** (2008) 877–898.